Hindawi
Advances in Civil Engineering
Volume 2023, Article ID 4176805, 17 pages
https://doi.org/10.1155/2023/4176805

Research Article

Novel Use of Scanning Methods to Investigate the Performance of Screw Connections in Timber-Concrete Composite Structures

Mohd Amirul B. Mohd Snin and Moustafa Moufid Kassem

School of Civil Engineering, Engineering Campus, Universiti Sains Malaysia, 14300 Nibong Tebal, Penang, Malaysia

Correspondence should be addressed to Mohd Amirul B. Mohd Snin; ceamirul@usm.my

Received 8 February 2023; Revised 15 May 2023; Accepted 27 May 2023; Published 3 June 2023

Academic Editor: Chayut Ngamkhanong

This paper investigates the shear force capacity, stiffness, and effective length of the connection screws in timber-concrete composite structures. Ten samples (six hardwood and four softwood) were fabricated with the connection screws installed at different angles through the interface. The shear force capacities and the global stiffness characteristics of the connections were determined directly from double shear tests. The local characteristics of the screw connections were investigated by scanning the final residual screw shapes at the end of the tests for softwood specimens. Using the 2D digital scans of the screws, the screw curvatures were determined. From the curvatures, the local distribution of moment along the screw embedded within the concrete at the conclusion of the test was estimated. The distance of the plastic hinge in the screw within the concrete from the interface between the concrete and timber (the effective length) was obtained from the maximum bending moment location calculated via this image scanning method. Empirical equations of effective screw length were developed from the test data and applied in a shear force capacity model for softwood. These new equations of effective length of inclined screws in connections predicted the shear force capacity of the connection better on the softwood specimens. In hardwood specimens, the screw failed in snapping. An equation of shear force capacity was developed based on the influence of the inclination angle of the screw with the reduction factors and can predict the shear capacity of the connection in hardwood specimens.

1. Introduction

Timber-concrete composite (TCC) systems are used in a variety of applications including flooring systems for multistory buildings and bridge decks [1–7]. TCC makes use of the concrete to resist compression and the timber to carry tension [8, 9]. The stiffness and strength of TCC structural systems in flexure are dependent on the performance of the shear connectors [10–13]. If these shear connectors do not perform well, large deflections and deformations will manifest in the structural system and potentially cause safety and serviceability failures [14–17]. Many types of shear connections can be used, such as glued joints [18] and mechanical fasteners (e.g., screws, steel dowels, notches, and plates) [19]. For more information on TCC structures, we see the state-of-the-art review articles by Yeoh et al. [2] and De Araujo et al. [20]. This study investigates the global shear performance of screwed connections in TCC. Eurocode 5 (EC5) is often used as a guide for those wishing to design screw connections in TCC structures [21]. However, there are limitations in the guidance given in EC5 with respect to TCC structures, as the formulations for predicting shear force capacity in connections in single and double shear (Figure 1(a)) are based on data from timber-timber (T-T) connections, as shown in equations (1) and (2) (formulations presented in CEN [21] EC5 cl. 8.2.2). There is also no consideration of the effect of plastic hinges on the screw in the basic formulation of shear force capacity for the screw connection.

For a fastener in a T-T system in single shear,

$$F_V = \min \begin{cases} f_{h,1,k} t_1 d, \\ f_{h,2,k} t_2 d. \end{cases} \quad (1)$$

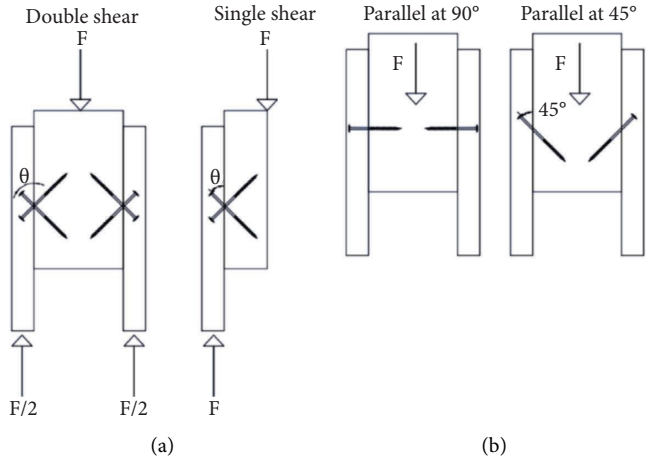

Figure 1: (a) Double shear versus single shear ; (b) parallel cases (45° and 90°).

For a fastener in a T-T system in double shear,

$$F_V = \min \begin{cases} 0.5 f_{h,1,k} t_1 d, \\ 0.5 f_{h,2,k} t_2 d, \end{cases} \quad (2)$$

where F_V = shear force capacity; $f_{h,1,k}$ = embedment strength for middle timber; $f_{h,2,k}$ = embedment strength for edge timber member; t_1 = thickness of middle timber; t_2 = thickness of edge timber; and d = screw diameter.

We note that a small number of previous research studies have attempted to predict mechanical properties of screw-based timber-concrete composite shear connectors. Symons et al. [11] discussed a model to calculate the slip moduli of inclined screw timber-concrete composite connections, assuming that the screw behaves as a beam on a 2-D elastic foundation with negligible deformation within the concrete. In a separate study, Symons et al. [12] presented an upper bound plastic collapse predictive model for screw connections strength, assuming that the screws behave perfectly plastically, and the concrete remains undamaged. Research by Moshiri et al. [22] also introduced a predictive model for the screw connection strength in crossed or X-formation where the screws resist shear tension and shear compression stresses, while the concrete remains undamaged. In 2020, Du et al. [23] proposed the stiffness model of the inclined screw connection in timber-concrete structures. The model was developed by assuming that the concrete remained undamaged. The screw connector within the timber and concrete was modelled as a semiinfinite beam method and included the inclination angle in the stiffness model. Mirdad and Chui [24] proposed the stiffness prediction of the timber-concrete composite connection with inclined screws and a gap. In their stiffness prediction model, all the assumptions and the early hypotheses were focused on the local characteristics of the screws embedded within the timber. The models were developed without any significant effect on the screw embedded within the concrete. Mirdad and Chui [24] also proposed analytical models of the shear strength of the screw connections within the timber to the concrete. Mirdad and Chui's models used the basis of Johansen's theory in their models to come up with the model that was able to estimate the strength of the inclined screw connection in the timber to concrete structures. This model also ignores any significant effect of the concrete on the embedded screw. In summary, EC5 and the predictive models from previous works all ignored any significant effect of the concrete on the connection behaviour.

Based on Gelfi et al. [25], the embedment strength of the screw embedded within the concrete is influenced by the effective length of the screw. The effective length of the screw is the distance of the hinge in the screw from the interface between the concrete and timber. However, the model proposed by Gelfi et al. [25] is limited to a screw angle of 90°. For screws at other angles, the distance of the hinge from the interface between the concrete and timber may also have a significant effect on the shear force capacity of the screw connection. It is also expected that the distance of the hinge from the interface between the concrete and timber is influenced by the screw angle. To obtain the value of embedment strength for the screw embedded within the timber, the formulations from CEN [21] EC5 clause 8.3.1.1) were used as shown in equation (3) (for softwood) and 4 (for hardwood). While to obtain the embedment strength for screws embedded within the concrete ($f_{h,c}$), the formula of embedment strength from the ACI-318 standard can be used and shown in equation (5) [26]:

$$f_{h,t} = 0.082 \rho_k d^{-0.3} \text{ (MPa) [for softwood]}, \quad (3)$$

$$f_{h,t} = 0.082 (1 - 0.01d) \rho_k \text{ (MPa) [for hardwood]}, \quad (4)$$

$$f_{h,c} = 0.85 f_c, \quad (5)$$

where ρ_k = density of timber and f_c = concrete strength.

In predicting the shear force capacity of the screw connections with various angles, the estimation does not only rely upon force due to the embedment strength (F_h). The strength of the shear force capacity also came from the withdrawal strength of the screw (F_{ax}) embedded within the concrete and timber. The combination of embedment strength and withdrawal strength of the screw is the total

shear force capacity of the screw connection (equation (6)). The formula to calculate force due to embedment strength in this study is shown in equation (7) which is also based on the EC5 code [21]. The formula for the withdrawal strength of the screw embedded within the timber can be obtained by using equation (8) (in timber) and equation (9) that are taken from the EC5 [21]. The withdrawal strength of the screw embedded within the concrete can be determined by using equation (8) (in concrete) and equation (10) (bond stress between concrete and screw) which are adapted from Eurocode 2 (EC2) [27]

$$F_v = F_h + F_{\mathrm{ax}}, \tag{6}$$

$$F_h = \begin{cases} f_{h,t} l_t d \ (\text{in timber}), \\ f_{h,c} l_c d \ (\text{in concrete}), \end{cases} \tag{7}$$

$$F_{ax} = \begin{cases} f_{\mathrm{ax}(t)} \mathrm{d}L_t \ (\text{in timber}), \\ f_{\mathrm{ax}(c)} \pi \mathrm{d}L_c \ (\text{in concrete}), \end{cases} \tag{8}$$

where

$$f_{\mathrm{ax}(t)} = 2 \times 10^{-6} \times \rho_k{}^2, \tag{9}$$

$$f_{\mathrm{ax}(c)} = 0.22 f_c. \tag{10}$$

Post-test observations of inclined screw TCC connections reported by Sebastian et al. [28] suggested that the screws can deform quite significantly in the concrete under longitudinal shear loading as shown in Figure 2. Therefore, in this research, the local deformation characteristics of the screws themselves were studied to better understand the global performance of TCC systems. The data from two series of TCC shear test specimen tests, one set using hardwood and the other using softwood, are combined in this paper. A novel scanning method was then used to analyse the deformed shapes of the screws at the end of the softwood tests and determine the effective length of the screws embedded in the concrete.

The main aim of this study was to combine data from two series of timber-concrete composite connection tests, one series using hardwood and one using softwood, and to develop a model to predict the interface capacity. The secondary aim of the research was to determine the local bending moment distributions along the screw connectors in timber-concrete composite structures. For further information on the results of this experimental program and the experimental methodology, we need to see Ducas [19] and Bin Mohd Snin [29].

2. Experimental Methodology

2.1. Specimen Fabrication. In the first series of tests, six double-shear hardwood (Bauchee) specimens were constructed. This was later followed by a second series of tests on four double-shear softwood (Spruce) specimens. In both cases, the specimens had a variety of screw inclination angles θ. The screws were generally installed in an X-formation (as shown in Figure 3) to ensure tension and compression that were developed when a shear force was applied to the specimen, except for three cases where parallel fasteners (at either 45° or 90° angles) were used.

The screw fasteners used in this work were partially threaded (PT) screws, 6 mm in diameter and 210 mm long. When installing the screws in the hardwood specimens, predrilling was required, but this was not necessary for the softwood specimens. Table 1 shows the identification codes for the tested specimens, the inclination angle, and the formation of the screws. The location of the screws and geometry of the specimens are shown in Figure 3.

2.2. Material Properties. Tensile testing was performed on a single screw according to ASTM [30]. Figure 4 shows the stress-strain curve obtained from this testing. Young's modulus of the screw fastener was calculated from the slope in the linear zone of Figure 4 as 222.9 GPa. Table 2 shows the interpolation functions fitted to the data for the "linear zone," "plastic zone," and "strain hardening zone." These functions were used in the subsequent analysis to calculate the stresses across the screw in both compression and tension (Section 4.2). Table 3 shows the results of the ASTM [31] tests on cylindrical specimens of the concrete used in the experimental work.

2.3. Double Shear Test Setup. Two potentiometers, Figure 5(c), were installed on the timber at the locations shown in Figure 5(b), to measure the slip between the concrete and timber. All the specimens were tested using a 500 kN capacity Dartec-2420 machine (1998 model), Figure 5(a), in displacement control (1 mm/min). Boundary conditions of a pinned support on one side of the specimen and a roller support on the other side (Figure 5(b)) were used to help eliminate the friction between the timber and the concrete when the test was running and thus avoided any frictional effects contributing to the measured shear force capacity. Data logging was conducted using a Visha 8000_3 at a sampling rate of 10 Hz. Testing was continued until the specimens showed significant signs of failure (e.g., concrete cracking or a loud breaking noise).

3. Shear Force Capacity and Slip Modulus

BSI [32] gives the following equation for calculating the global stiffness (Ks) for TCC structures:

$$K_{s,n} = \frac{n F_{v,\max}}{\delta_n}, \tag{11}$$

where $n = 0.4$ or 40 (serviceability limit state), 0.6 or 60 (ultimate limit state), and 0.8 or 80 (which is used to calculate the ductility, see: Stehn and Johansson [33], and where $F_{\mathrm{v,max}}$ = maximum load and δ_n = displacement of the connection at the particular point.

The results of shear force capacity against displacement for all the tests are shown in Figure 6. The maximum shear capacities from the plots were used to investigate the local characteristics of the screws later in this paper. Table 4 summarises the test results, giving the measured stiffness

(a) (b)

Figure 2: Plastic deformation of inclined screws in timber-concrete composite connections: (a) near concrete-timber interface; (b) near head of screw in concrete [28]. Reprinted from construction and building materials, 102, W. M. Sebastian, J. Mudie, G. Cox, M. Piazza, R. Tomasi, and I. Giongo, insight into the mechanics of externally indeterminate hardwood-concrete composite beams, 1029–1048, copyright (2018), with permission from Elsevier.

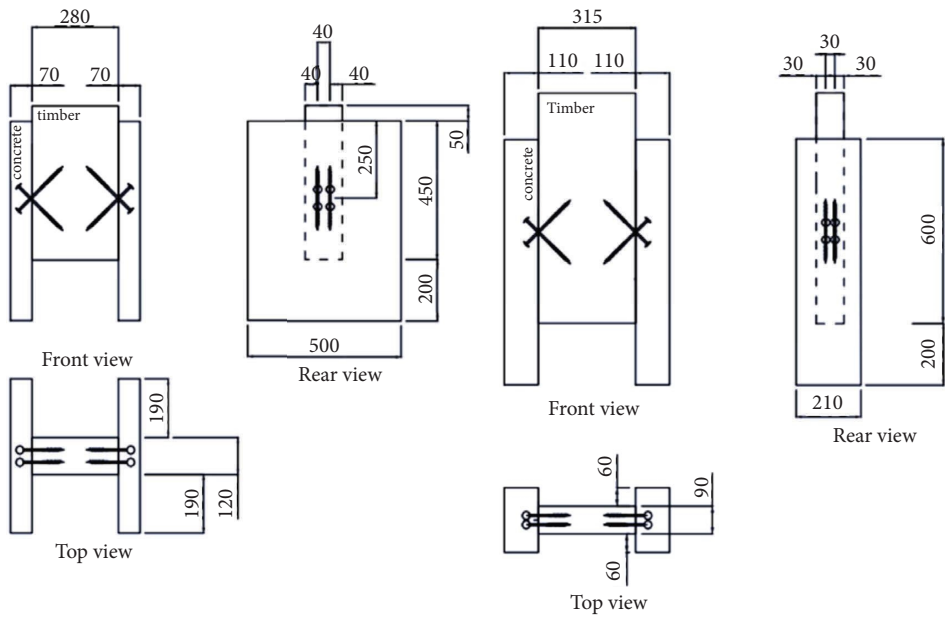

Figure 3: Typical screw formation and specimen dimensions of (a) hardwood and (b) softwood.

Table 1: Specimen nomenclature.

Specimen	Inclination angle (°)	Screw formation
X30h	30	X
X45h	45	X
X60h	60	X
X75h	75	X
P90h	90	P
P45h	45	P
X45s	45	X
X60s	60	X
X75s	75	X
P90s	90	P

X = X formation; P = Parallel; h = hardwood; s = softwood.

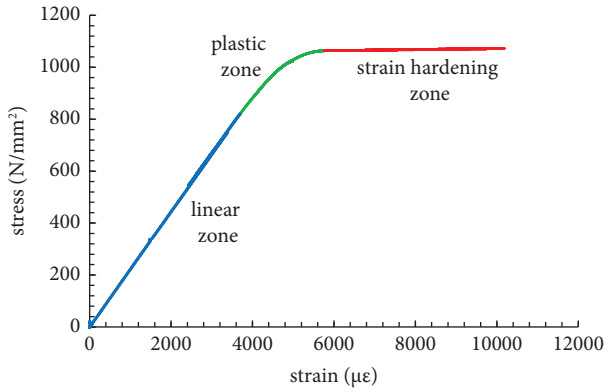

Figure 4: Measured stress-strain curve of a tension test on a single screw.

Table 2: Interpolation functions fitted to the measured stress-strain data for a single screw.

Zone	Fitted equation	Applicable range (positive values indicate tension)
Linear zone	$\sigma_{si} = E_s\varepsilon_{si}$	$-3695 < \varepsilon_{si} < 3695$
Plastic zone	$\sigma_{si} = -5.7 \times 10^{-5}\varepsilon_{si}^2 + 0.66\varepsilon_{si} - 849.76$	$-5763 < \varepsilon_{si} < -3695$ and $3695 < \varepsilon_{si} < 5763$
Strain hardening zone	$\sigma_{si} = 2 \times 10^{-3}\varepsilon_{si} + 1052.2$	$\varepsilon_{si} < -5763$ and $5763 < \varepsilon_{si}$

Table 3: ASTM [31] C39 test results on cylindrical specimens for use in the experimental program. Mix 1 was used for the hardwood tests, and mix 2 was used for the softwood tests.

	Mixture proportion			T1 (N/mm^2)	T2 (N/mm^2)	T3 (N/mm^2)	Average (N/mm^2)
	Cement	Sand	Aggregate				
Mix 1	1	1	2	26.00	26.60	26.80	26.5
Mix 2	1	2	4	16.49	16.08	16.52	16.36

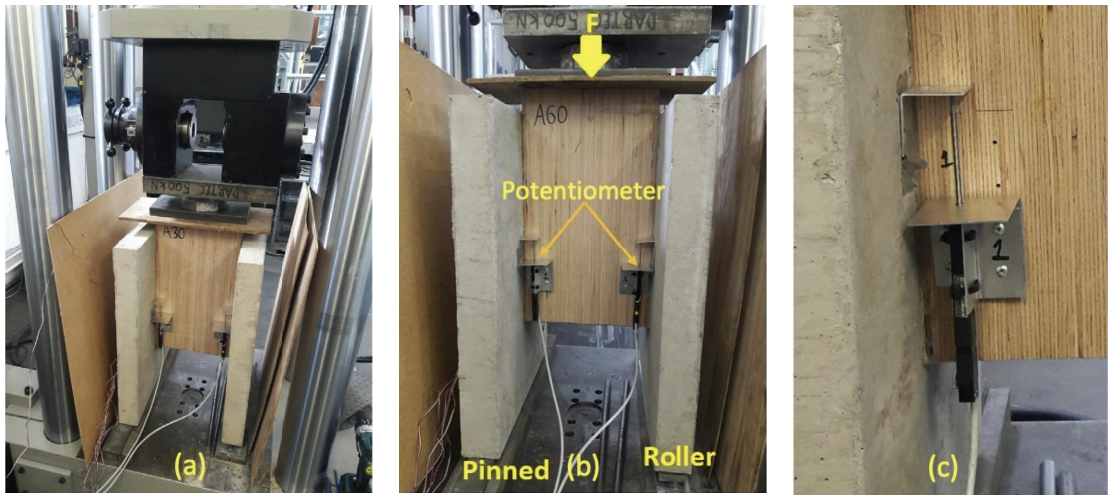

(a) (b) (c)

Figure 5: Double shear test set up (photos: author).

(using equation (11)) and shear force capacity (capacity per side) for the ten specimens.

For the hardwood specimens, specimen X45 h exhibited the stiffest connection at 74.4 kN/mm, 70.9 kN/mm, and 64.3 kN/mm for K_{s40}, $K_{s60,}$ and $K_{s80,}$ respectively. The relatively small variation in these values indicates that there was relatively little nonlinear behaviour. For the softwood specimens, X45 s exhibited the stiffest connection at 37 kN/mm, 26.8 kN/mm, and 18.3 kN/mm for K_{s40}, $K_{s60,}$ and $K_{s80,}$ respectively. Overall, when the screws were inclined at 45°,

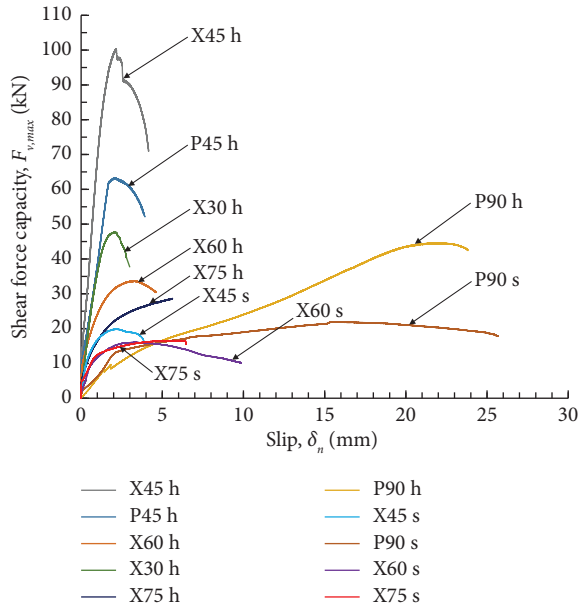

Figure 6: Shear force capacity versus slip.

the stiffness of the connection was at its greatest. For further analysis of the screws, shear force capacities were divided by two to obtain the maximum shear force capacity in a single screw. The failure mode of the hardwood specimens was observed, and it shows that the screw was snapped as shown in Figure 7 for specimens P45 h and P90 h.

From this observation, the higher concrete grade (Mix 1 : 26.5 MPa) in hardwood specimens causes the connection to fail as it snaps at the screw between the interface of concrete and timber. For this reason, a batch of the lower concrete grade (Mix 2 : 16.36 MPa) to the timber specimen was fabricated to see the significant effect of the concrete on the location of the plastic hinge on the screw in the specimens. Compared to the hardwood specimens, the connections in the softwood specimens failed in a ductile manner (Figure 8). During the tests, the screws engraved the timber to make the channels. At this time, the slip of the screw connections in softwood specimens increased more than in hardwood specimens. This situation makes the screw connections in softwood specimens behave in a ductile manner. Meanwhile, the screw embedded in the concrete remained in its original position with some deformation. The main reason for this situation happening in the timber is due to its low density and flexural strength. The length of the channels made by the screw depended on the screw inclination fitted to the specimen. Figure 8 also shows the different lengths of channels caused by the screw according to the angles of 45, 60°, 75°, and 90°. It was found that the channel length decreased when the angle of the screw decreased from 90° to 45°. This suggests that in practice, the 90° screw will produce more significant deformation compared to its other inclined counterparts.

3.1. Theoretical of the Hardwood Connection Failure Mode. Screw connections in hardwood specimens failed as they snapped on the screw. This failure mode can be implicated from Figure 9 where the shear force capacity of the connection is calculated based on the shear stress of the cross-sectional area of the screw. Variety in the inclination angles may influence the total cross-sectional area of 90° to 30° specimens (equation (12)).

This shows that the influence of the angle will change the value of d' as shown in equation (13). In order to determine the cross-sectional area of the screw, we utilize the oval area equation, as indicated in equation (12). For hardwood samples, the shear force capacity of the connection can be given as equation (14). Based on the RCSC [34], nominal shear strength of the bolt is expressed as in equation (15).

Normally, the shear strength of the bolt is 60% of the tensile strength. In RCSC [34], it was suggested that the shear strength of the bolt τ_s is taken as 0.625 of the tensile strength of the bolt $\sigma_{y(s)}$. Reduction factor C_a (0.75) is applied on equation (14) due to nonuniform force distribution between bolts and in a long joint and the minor second-order effects such as those resulting from the action of the applied loads on the deformed structure should be accounted for through a second-order analysis of the structure RCSC [34]. Another reduction C_b (0.8) is applied to the shear strength to account for the reduction in shear strength for a bolt with threads included in the shear plane but calculated with the area corresponding to the nominal bolt diameter (RCSC). Finally, the shear force capacity of the connection in a hardwood specimen can be obtained from equation (16). This shear force capacity indicates the strength of the connection in the hardwood-concrete specimens given as follows:

Table 4: Slip modulus of connection per side based on the 5 mm maximum slip.

Specimen	Angle (°)	Slip modulus at 40% of maximum load, $K_{s,40}$ (kN/mm)	Slip modulus at 60% of maximum load, $K_{s,60}$ (kN/mm)	Slip modulus at 80% of maximum load, $K_{s,80}$ (kN/mm)	Shear force capacity $F_{v,max}$ (kN)
X30h	30	41.0	39.6	35.2	47.5
X45h	45	74.4	70.9	64.3	100.0
X60h	60	51.7	29.6	20.9	33.5
X75h	75	25.0	15.7	10.3	28.5
P90h	90	6.6	3.5	3.9	44.5
P45h	45	43.6	38.1	37.6	63.0
X45s	45	37.0	26.8	18.3	19.9
X60s	60	18.1	15.5	10.0	16.0
X75s	75	25.4	16.8	10.3	16.4
P90s	90	6.1	6.2	6.3	16.1

(a) (b)

Figure 7: Snapped screw remained in the concrete and timber (a) specimen P90h (b) specimen P45h (photo: author).

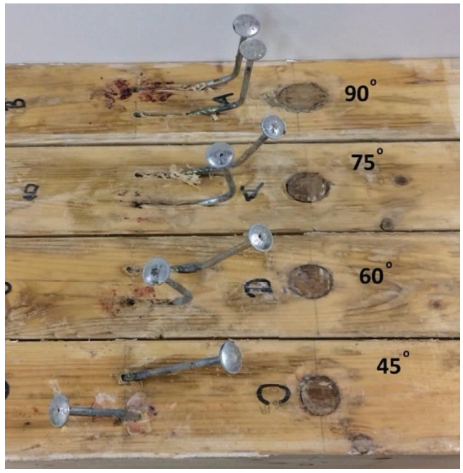

Figure 8: Channels length made by an inclined screw at different angles (photo: author).

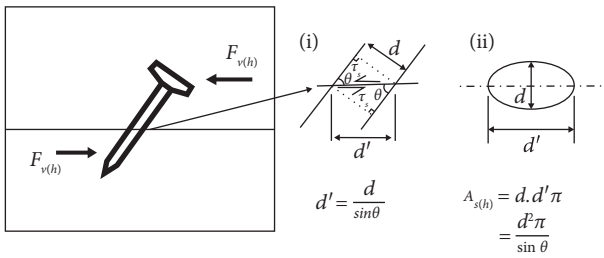

Figure 9: Influence of the inclination angle on the total cross-sectional area.

$$A_{s(h)} = d.d^{'}.\pi, \tag{12}$$

$$d^{'} = \frac{d}{\sin\theta}, \tag{13}$$

$$F_{v(h)} = \frac{\tau_s d^2 \pi}{\sin\theta}, \tag{14}$$

$$F_{v(h)} = 0.625 C_a C_b \frac{\sigma_{y(s)} d^2 \pi}{\sin\theta}, \tag{15}$$

$$F_{v(h)} = 0.375 \frac{\sigma_{y(s)} d^2 \pi}{\sin\theta}. \tag{16}$$

4. Local Behaviour of Screw Connections in Softwood TCC

4.1. Generation 2D View of Screws from Coordinates. Using the results from sample X45s, an example of how the bending moment distribution along the screw embedded within the concrete was established is shown as follows. This novel scanning method was used to determine the bending along the full length of the screws at the end of the tests.

At the completion of testing, the screws were cut out of the test specimens as carefully as possible to minimize any changes or variations in the screw displacements. A portable coordinate measuring machine (CMM) scanner (a FARO Model 14000 3D scanner) was then used to measure the screw shapes at the end of the tests. The coordinates obtained from the CMM scanner were imported into MATLAB to create the scanned images shown as a two-dimensional view in Figure 10.

These scans were then analysed further to extract the distorted shapes of each screw (e.g., Figure 11). Figure 10(a) shows that the tension screw in specimen X45s (the leftmost screw) has no hinges along the section embedded within the concrete (the section towards the head of the screw). However, it was found that a hinge did occur in the other tension screws, and the location of this hinge moved closer to the screw head as the screw angle increased. It was also found that only a single hinge occurred in the part of the screw embedded within the concrete. Figure 10(b) shows the scanned image for the compression screws. The top hinge in the 45° screw was closer to the screw head compared to that in the screws in the other specimens. The hinges in the compression screws occurred when the screw was being compressed in the concrete, and this resulted in more significant curvatures compared to the tension screws. The top

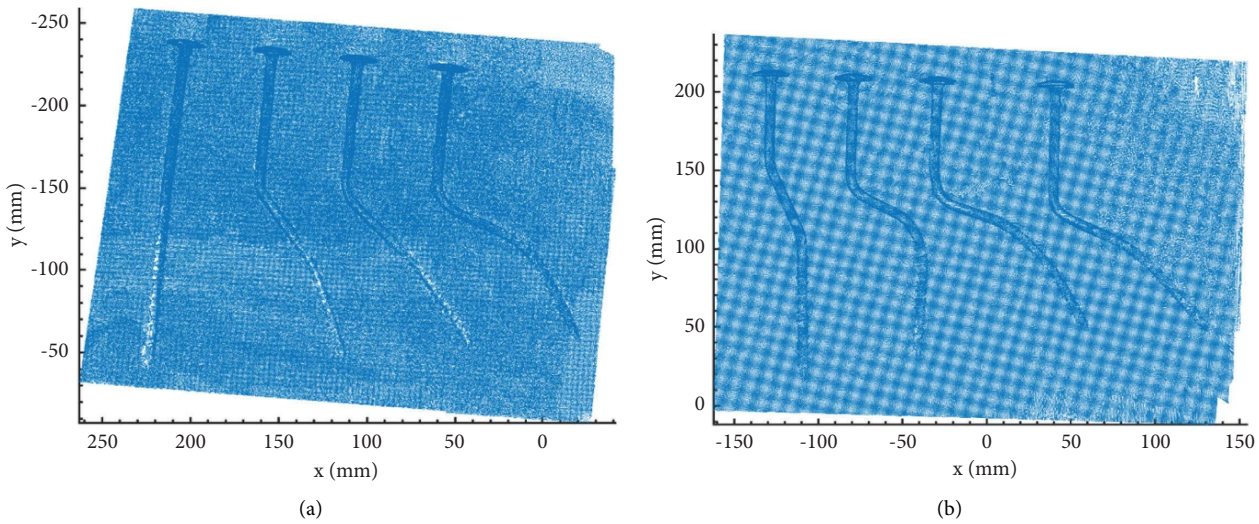

Figure 10: Scanned images of softwood specimens: (a) tension screws in 45°, 60°, 75°, and 90°; (b) compression screws in 45°, 60°, 75°, and 90°.

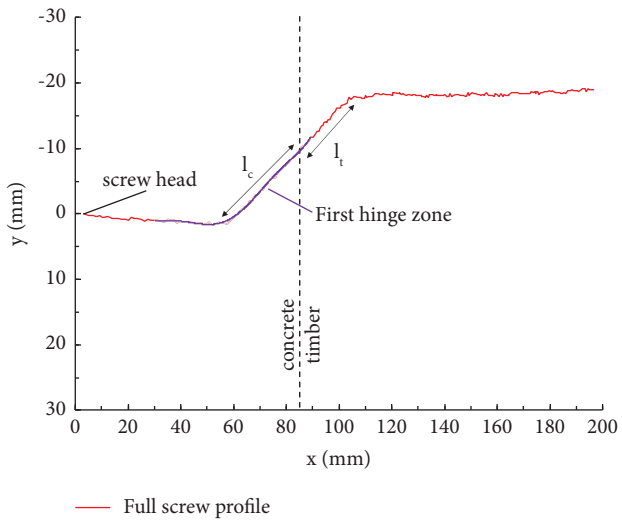

Figure 11: Plot of the tested compression screw in *x*-*y* axis for X45s.

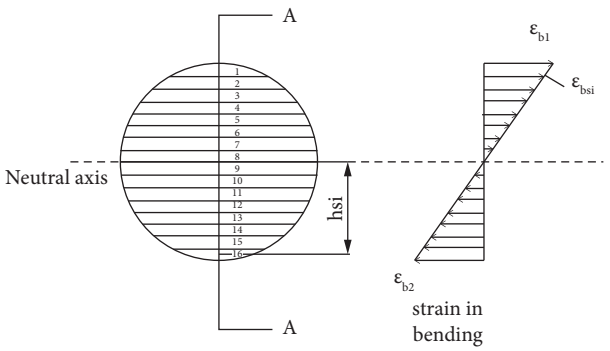

Figure 12: Strip fibre analysis of a screw.

hinge was located further away from the screw head as the angle of the compression screw increased from 45° to 90°. This was the reverse of the change in the tension screw hinge location, which got closer to the screw head as the screw angle increased.

4.2. Analysis of the Scanned Coordinate Data for the Compression Screw (X45s). Figure 11 shows the extracted deformation data for the compression screw in specimen X45s. The curvature formula given in equation (17) was then used to determine the curvature at every point along the length of the screw.

$$k = \frac{y''}{\left(1 + y'^2\right)^{3/2}}. \tag{17}$$

For the compression screw in specimen X45s, the maximum curvature was $-0.002\,\text{mm}^{-1}$ and the distance of the plastic hinge from the timber-concrete interface was calculated as 22.5 mm. The value of curvature obtained is useful as it can be used to calculate the fibre strains across the screw section (Figure 12).

By knowing the distance of the edge fibre to the middle of the screw (hsi), it is possible to find the extreme fibre stress ($\varepsilon b2$) using the following equation:

$$\varepsilon_{b2} = k.h_{\text{si}}. \tag{18}$$

Unfortunately, it was not possible to measure the change in diameter of the screw when the deformation was plastic; thus, the curvatures during plastic deformation were also calculated using equation (18). For the value of max curvature in the screw within specimen X45s, the max strain was calculated as −0.006.

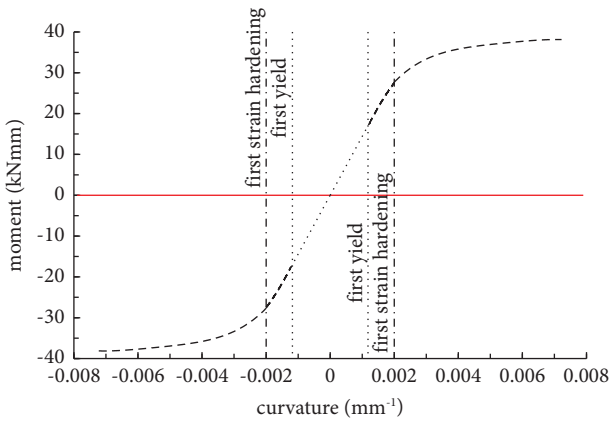

Figure 13: Bending moment vs. curvature of a screw.

The local bending moments along the screw length embedded within the concrete were also obtained from the measured curvatures. To allow the local bending moments to be calculated when the screw had reached a plastic or strain hardening phase, a plot of moment against curvature was produced as shown in Figure 13 and based on equations (19)–(21). This plot incorporates the nonlinear stress-strain curve (Figure 4 and Table 2) and uses a strip analysis method. The figure was created by calculating the stress profile for every curvature, then for each strip across the section, using the relevant moment equations equations (19)–(21) and summing the values for all the strips to get the total section bending moment. Figure 13 was then used to convert the curvatures into moments at every point along the screw length embedded within the concrete as follows:

$$M_{s(E)} = \int kE_s h_{si}^{\,2}\,\mathrm{dA_{si}}, \tag{19}$$

$$M_{s(P)} = \int \left(-5.7\times10^{-5}\left(\mathrm{kh_{si}}\right)^2 + 0.66kh_{si} - 849.76\right)h_{\mathrm{si}}\,\mathrm{dA_{si}}, \tag{20}$$

$$M_{s(\mathrm{SH})} = \int \left(2\times10^{-3}kh_{si} + 1052.2\right)h_{\mathrm{si}}\,\mathrm{dA_{si}}. \tag{21}$$

5. Bending Moment Distributions and Hinge Locations along the Screws

5.1. Bending Moment Distributions. Figure 14 shows the local bending moment distribution for the compression screws embedded within the concrete in specimens X45s, X60s, and X75s calculated using the method mentioned previously.

5.2. Plastic Hinge Locations. Using the scanned shape of the screws at the end of the tests, it was also possible to accurately determine the location of the plastic hinges in the screws (Figure 11 for location of plastic hinges l_c and l_t) Tables 5 and 6 show computed plastic hinge locations. The distance of the plastic hinge in concrete and timber from the timber-concrete interface is named $l_{c(\mathrm{scan})}$ and $l_{t(\mathrm{scan})}$, respectively. Tables 5 and 6 also show an increasing distance for the location of the plastic hinge from the timber-concrete interface as the angle of the compression screw reduces from 90 to 45 degrees. But with the tension screw embedded within the concrete, the location of the plastic hinge at the timber-concrete interface decreased as the angle of the screw reduced from 90 to 45 degrees. Contrary to the tension screw embedded within the timber, the distance location of the plastic hinge from the timber-concrete interface increased as the angle of the screw reduced from 90 to 45 degrees.

To calculate the shear force capacity of the interface, the embedment strength of the screw must be calculated. Based on Gelfi et al. [25], the embedment strength of the screw within the concrete is the concrete bearing stress multiplied by the effective length l_c. However, the model presented by Gelfi et al. [25] was developed only for screws at an angle of 90°. These new tests extend this previous work by allowing an investigation of the effective length of the screw in the concrete and timber for different screw angles. The ratio between the plastic hinge distance $l_{c(\mathrm{scan})}$ and the length of the fastener in concrete L_c is defined as the plastic hinge ratio $\varnothing_{Hc}$ (equation (22)). The distance of plastic hinge from the timber-concrete interface is used to quantify the effective length of the screw l_c. A plot of the plastic hinge ratio against the angle of the screw in concrete is shown in Figure 15 to investigate the effect of the screw angle on the plastic hinge distance. Figure 15 shows that for fasteners in compression, the plastic hinge ratio decreases when the angle increases from 45 to 90 degrees and increases for fasteners in tension when the angle increases from 45 to 90 degrees. Using a linear fit to the data presented in Figure 15, equations for plastic hinge ratio for the fasteners in tension and compression, respectively, are presented in the following equations:

$$\varnothing_H = \frac{l_c}{L_c} \text{ or } \frac{l_t}{L_t}, \tag{22}$$

$$\varnothing_{\mathrm{Hc}(t)} = 0.0031\theta - 0.11 \text{ (screw in tension)}, \tag{23}$$

$$\varnothing_{\mathrm{Hc}(c)} = 0.50 - 0.0040\theta \text{ (screw in compression)}, \tag{24}$$

l_c can be determined, as shown in equations (25) and (26), respectively. These equations for l_c can then be used to calculate the shear force capacity of the interface.

For tension screw (for the softwood tests),

$$l_c = 0.0031\theta L_c - 0.11L_c. \tag{25}$$

For compression screw,

$$l_c = 0.50L_c - 0.0040\theta L_c. \tag{26}$$

The plot of the plastic hinge ratio against the angle of the screw in timber was also made and shown in Figure 16. Figure 16 shows that the plastic hinge ratio for fasteners in compression decreases when the angle increases from 45 to 90 degrees. From the plot, the equations for the plastic hinge

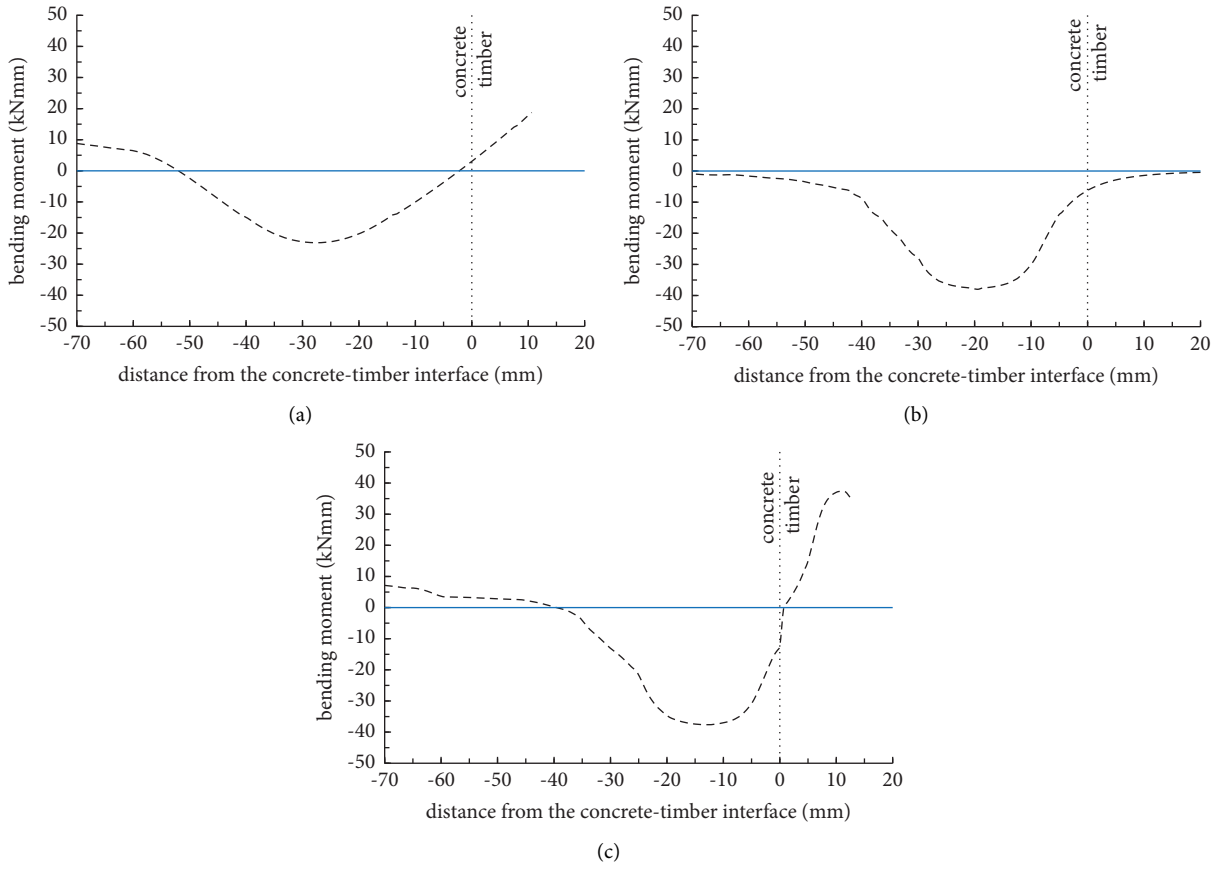

Figure 14: Bending moment along the compression screw for (a) specimen X45s, (b) specimen X60s, and (c) X75s at the end of tests.

Table 5: Plastic hinge locations from the scanning method (in concrete).

Specimen	Angle	$l_{c(\text{scan})}$ (mm)		L_c (mm)	$\phi_{Hc} = l_{c(\text{scan})}/L_c$	
		Compression	Tension		Compression	Tension
X45s	45	26	1	85	0.31	0.01
X60s	60	21	7	85	0.25	0.08
X75s	75	15	11	85	0.18	0.13
X90s	90	12	12	85	0.14	0.14

$l_{c(\text{scan})}$ = plastic hinge distance from the timber-concrete interface. L_c = length of the fastener embedded within the concrete.

Table 6: Plastic hinge locations from the scanning method (in timber).

Specimen	Angle	$l_{t(\text{scan})}$ (mm)		L_t (mm)	$\phi_{Ht} = l_{t(\text{scan})}/L_t$	
		Compression	Tension		Compression	Tension
X45s	45	20	45	125	0.25	0.56
X60s	60	14	35	125	0.18	0.44
X75s	75	10	30	125	0.13	0.38
X90s	90	5	0	125	0.06	0

$l_{t(\text{scan})}$ = plastic hinge distance from the timber-concrete interface. L_t = length of the fastener embedded within the concrete.

ratio for compression and tension are shown in the following equations:

$$\varnothing_{\text{Ht}(t)} = -0.0117\theta + 1.13 \text{ (Screw in tension)}, \quad (27)$$

$$\varnothing_{\text{Ht}(c)} = -0.0041\theta + 0.43 \text{ (Screw in compression)}. \quad (28)$$

l_t can be determined, as shown in equations (29) and (30), respectively. These equations can then be used to calculate the shear force capacity of the interface.

For the tension screw (for the softwood tests),

$$l_t = -0.0117\theta L_t + 1.13 L_t. \quad (29)$$

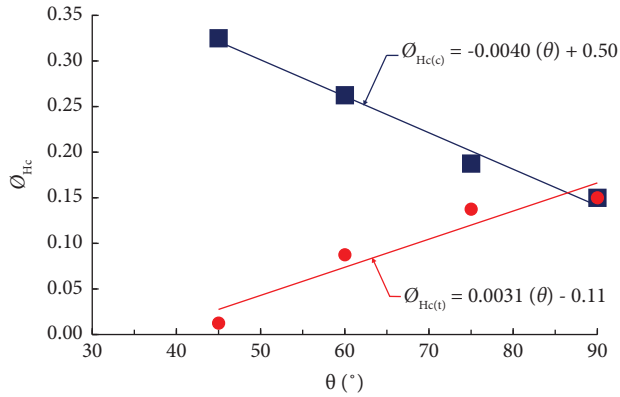

Figure 15: Plastic hinge ratio by the screw angle (in concrete).

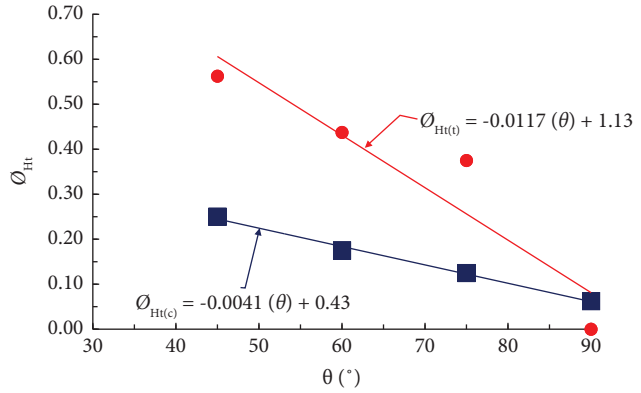

Figure 16: Plastic hinge ratio by the screw angle (timber).

Table 7: Degree of accuracy between equations (25) and (26) (l_c) for the screw in concrete.

Specimen	Angle	l_c (compression)			l_c (tension)		
		Scan (mm)	Equation (26) (mm)	Percentage different (%)	Scan (mm)	Equation (25) (mm)	Percentage different (%)
X45s	45	26	27.2	4.41	1	2.51	60.16
X60s	60	21	22.1	4.98	7	6.46	−8.35
X75s	75	15	17.0	11.77	11	10.41	−5.67
X90s	90	12	11.9	−0.08	12	14.37	16.49

Table 8: Degree of accuracy between equations (29) and (30) (l_t) for the screw in timber.

Specimen	Angle	l_t (compression)			l_t (tension)		
		Scan (mm)	Equation (30) (mm)	Percentage different (%)	Scan (mm)	Equation (29) (mm)	Percentage different (%)
X45s	45	20	30.69	34.83	45	75.45	67
X60s	60	14	23	39.13	35	53.65	53.28
X75s	75	10	15.31	34.68	30	31.56	5.2
X90s	90	5	7.63	34.47	0	9.625	100

For the compression screw,

$$l_t = -0.0041\theta L_t + 0.43L_t. \quad (30)$$

The degree of accuracy for equations (25), (26), (29), and (30) has been measured and shown in Tables 7 and 8. Table 7 shows the degree of accuracy for equations (25) and (26) for screws embedded within the concrete. It was found that the percentage difference between equation (26) (compression) to scanned values for all softwood specimens is less than 12%. The values calculated by using equation (25) (tension) are also compared to the scanned values and show that the percentage difference is less than 60%. However, the values

Table 9: Shear force capacity per screw predicted using effective length equations (25), (26), (29), and (30) for F_v (in concrete) and F_v (in timber) for softwood specimens, respectively.

Specimen	L_c (mm)	D (mm)	L_t (mm)	$f_{h,c}$ (MPa) Equation (5)	$f_{h,t}$ (MPa) (Equations (3)/(4))	$f_{ax,t}$ (MPa) Equation (9)	$f_{ax,c}$ (MPa) Equation (10)	l_c (mm) Equations (25)/(26)	l_t (mm) Equations (29)/(30)	(1) F_v (timber) (kN) Equation (6)	(2) F_v (concrete) (kN) Equation (6)	(3) F_{max} (measured) (kN)	(1)/(3)	(2)/(3)
X45s	85	6	125	14.14	20.12	3.53	3.66	27.2	30.69	6.35	11.10	9.94	0.64	1.12
X60s	85	6	125	14.14	20.12	3.53	3.66	22.1	23	5.42	10.66	8.01	0.68	1.33
X75s	85	6	125	14.14	20.12	3.53	3.66	17.0	15.31	4.49	10.23	8.21	0.55	1.25
X90s	85	6	125	14.14	20.12	3.53	3.66	11.9	7.63	3.57	9.80	8.05	0.44	1.22
												Mean	0.58	1.23
												Standard deviation	0.10	0.09
												Coefficient of variance	18.05	7.19

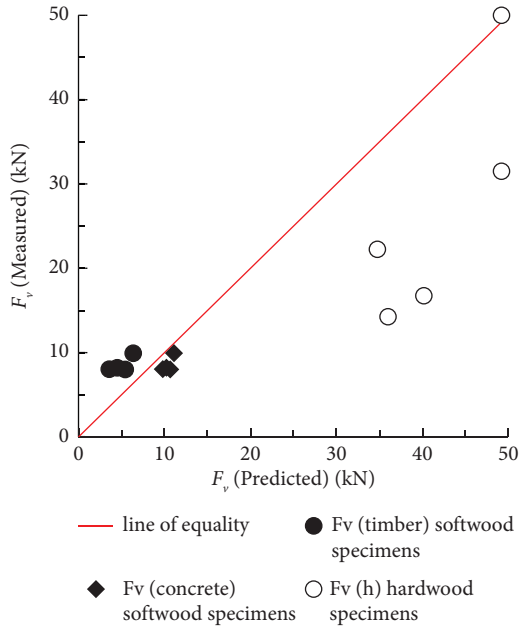

Figure 17: F_v (measured) versus F_v (predicted) (equation for effective length l_c and l_t [softwood] and equation (16) (hardwood) from this research).

Table 10: Shear force capacity per screw predicted using equation (16) for $F_v(_h)$ for the hardwood specimen.

Specimen	d (mm)	$\sigma_{y(s)}$ (MPa)	θ (°)	(1) $F_{v(h)}$ (concrete) (kN) Equation (16)	(2) F_{max} (measured) (kN)	(1)/(2)
X30h	6	820	57.04	69.55	23.75	2.93
X45h	6	820	57.04	49.18	50	0.98
X60h	6	820	57.04	40.15	16.75	2.40
X75h	6	820	57.04	35.99	14.25	2.53
P90h	6	820	57.04	34.76	22.25	1.56
P45h	6	820	57.04	49.18	31.5	1.56
					Mean	1.99
					Standard deviation	0.74
					Coefficient of variance	36.96

between both methods are not far from each other. For the screw embedded within the timber, three specimens have different percentages between equation (29) (tension) to the scanned values of more than 50%. Meanwhile, the percentage difference between equation (30) (compression) to the scanned values is around 35% for all softwood specimens. For future works, the additional samples can be fabricated and tested to improve the equation (25), (26), (29), and (30) accuracies.

5.3. Validation of the New Effective Length of Shear Force Capacity Equations. The new effective length formulations (equations (25), (26), (29), and (30)) were used to calculate interface shear force capacities (using equation (6)). Equations (25), (26), (29), and (30) (generated for softwood test data) were taken to be valid for the interpretation of the softwood tests. Table 9 shows the results of shear force capacity for both approaches of l_c and l_t calculations. Most of the values of shear force capacities calculated using this study's effective length equations were closer to the measured shear force capacities. This can be seen in Figure 17, where the softwood data obtained by the new equations (effective length l_c and l_t) are closer to the line of equality. Therefore, it is suggested that the effective length method proposed in this study is used when it is desirable to have a good prediction of the interface shear force capacity for the softwood specimens. Meanwhile, the hardwood data obtained by equation (16) (see Table 10) is quite overestimated from the line of equality. More reduction factors may need to be included in the proposed equation (16) to obtain more factors that influence the shear force capacity in hardwood specimens. This research suggests future work to discover insight into the local behaviour of the screw connections in hardwood specimens by investigating the local bending moment, axial load, and deformation along the screw within the specimens.

6. Conclusion

A set of ten double shear test specimens with different screw angles was tested. It was found that the specimens with the highest shear force capacity and stiffness were specimens X45 h and X45s for hardwood and softwood, respectively. The shear force capacity of the connections decreased when the screw angle increased to 90°. All these test results were then used to achieve the two main aims of the research. The first aim of this research is to develop a model to predict the interface capacity. From the results of the scanning method, a plastic hinge ratio is introduced to develop equations for the effective length based on the plot of the plastic hinge ratio for various screw angles. The use of four new equations (25), (26), (29), and (30) to calculate the effective length of the screws results in better overall prediction of the interface capacity for softwood. In the hardwood specimens, (16) we slightly overestimated the value of shear force capacity. However, the predicted value from equation (16) may be improved if factors such as the local bending moment, axial load, and deformation along the screw length are considered for future work. The second aim of this research is to determine the local bending moment distributions along the screw connectors in TCC structures. The local bending moments along the screws at the end of the testing were calculated from scans of the final shape of the screws. From the analysis of the curvature values obtained from the scanned image, the local bending moments were developed as shown in Figure 14. From Figure 14, the maximum bending moment along the screw length embedded within the concrete occurred at the location of the hinge. From that observation, the distance of the hinge from the interface between the timber and the concrete can be obtained from the maximum bending moment.

Notations

$A_{s(h)}$: Cross sectional area of the screw (oval shape equation)
D or d: Diameter of the fastener
dA_{si}: Area for each strip
C_a and C_b: Reduction factor in shear strength of the screw
E_s: Young's modulus of fastener
F_{ax}: Force due to withdrawal strength
F_h: Force due to embedment strength;
$F_{V(h)}$: Shear force capacity in hardwood specimens
F_V: Shear force capacity
$F_{v,\max}$: Maximum shear force capacity
$f_{ax,c}$: Bond stress between concrete to screw
$f_{ax,t}$: Characteristic point side withdrawal strength of the screw in timber
$f_{h,1,k}$: Embedment strength for middle timber from EC5
$f_{h,2,k}$: Embedment strength for edge timber member from EC5
$f_{h,t}$: Embedment strength of the screw within timber member
$f_{h,c}$: Embedment strength of the screw within concrete member
h_{si}: Distance from neutral axis
k: Curvature
$K_{s,40}$: Stiffness at serviceability state
$K_{s,60}$: Stiffness at ultimate limit state
$K_{s,80}$: Stiffness at 80% of the maximum shear force capacity
L_c: Fastener length embedded within the concrete
L_t: Fastener length embedded within the timber
l_c: Effective length of the screw embedded within the concrete
l_t: Effective length of the screw embedded within the timber
$l_{c(\text{scan})}$: Effective length of the screw embedded within the concrete for scanning method
M_s: Local bending moment
$M_{s(E)}$: Local bending moment in elastic range
$M_{s(P)}$: Local bending moment in plastic range
$M_{s(SH)}$: Local bending moment in strain hardening range
M_y: Yield moment of the fastener;
n: 0.4 (serviceability limit state), 0.6 (ultimate limit state) or 0.8 (which is used to calculate the ductility)
t_1: Thickness of middle timber from EC5
t_2: Thickness of edge timber from EC5
y: Lateral displacement of screw
y': First derivative of y
y'': Second derivative of y
β: The ratio between the concrete to timber embedment strength
δ_n: Displacement of the connection at particular point
ε_{bsi}: Bending strain
ε_{si}: Strip strain in the screw
ε_{b1} and ε_{b2}: Extreme fibre strains in the screw
θ: Angle of screw inclination
$\varnothing_H$: Plastic hinge ratio
$\varnothing_{Hc(c)}$: Plastic hinge ratio for compression screw in concrete
$\varnothing_{Hc(t)}$: Plastic hinge ratio for tension screw in concrete
$\varnothing_{Ht(t)}$: Plastic hinge ratio for tension screw in timber
$\varnothing_{Ht(c)}$: Plastic hinge ratio for compression screw in timber
ρ_k: Density of timber
σ_{si}: Strip stress in the screw
$\sigma_{y(s)}$: Yield strength of the screw
τ_s: Shear strength of the screw.

Data Availability

The data used to support the findings of this study are included within the article.

Disclosure

The manuscript was already published as a thesis based on the link https://research-information.bris.ac.uk/ws/portalfiles/portal/283844211/Final_Thesis_31.7.2021.pdf.

Conflicts of Interest

The authors declare that they have no conflicts of interest.

Acknowledgments

The first author acknowledges the funding received from the Ministry of Higher Education Malaysia and Universiti Sains Malaysia which helped fund his doctoral studies at the University of Bristol.

References

[1] M. Schmid, "Acoustic performance of timber concrete composite floors," in *Proceedings of the International Congress on Noise Control Engineering 2005 (INTERNOISE 2005)*, vol. 2, pp. 913–922, Rio de Janeiro, Brazil, August 2005.

[2] D. Yeoh, M. Fragiacomo, M. De Franceschi, and K. Heng Boon, "State of the art on timber-concrete composite structures: literature review," *Journal of Structural Engineering*, vol. 137, no. 10, pp. 1085–1095, 2011.

[3] A. M. P. G. Dias, M. C. P. Ferreira, L. F. C. Jorge, and H. M. G. Martins, "Timber-concrete practical applications-bridge case study," *Proceedings of the Institution of Civil Engineers - Structures and Buildings*, vol. 164, no. 2, pp. 131–141, 2011.

[4] H. Svatoš-Ražnjević, L. Orozco, and A. Menges, "Advanced timber construction industry: a review of 350 multi-storey timber projects from 2000–2021," *Buildings*, vol. 12, no. 4, p. 404, 2022.

[5] A. Bahrami, J. Jakobsson, and T. Söderroos, "Factors influencing choice of wooden frames for construction of multi-story buildings in Sweden," *Buildings*, vol. 13, no. 1, p. 217, 2023.

[6] E. Martín-Gutiérrez, J. Estévez-Cimadevila, F. Suárez-Riestra, and D. Otero-Chans, "Flexural behaviour of a new timber-concrete composite structural flooring system. Full scale testing," *Journal of Building Engineering*, vol. 64, Article ID 105606, 2023.

[7] Z. Li and K. D. Tsavdaridis, "Design for seismic resilient cross laminated timber (clt) structures: a review of research, novel connections, challenges and opportunities," *Buildings*, vol. 13, no. 2, p. 505, 2023.

[8] J. Natterer, J. Hamm, and P. Favre, "Composite wood-–concrete floors for multistory buildings," *Proceedings of the International Wood Engineering Conference*, vol. 3, pp. 431–435, 1996.

[9] A. Ceccotti, "Composite concrete-timber structures," *Progress in Structural Engineering and Materials*, vol. 4, no. 3, pp. 264–275, 2002.

[10] M. Patrick, D. Dayawansa, and R. Wilkie, *Design of Simply - Supported Composite Beams for Strength (To Australian Standard AS 2327.1-1996)*, Onesteel Manufacturing Limited, Sydney, Australia, 2nd edition, 2001.

[11] D. Symons, R. Persaud, and H. Stanislaus, "Slip modulus of inclined screws in timber-concrete floors," *Proceedings of the Institution of Civil Engineers – Structures and Buildings*, vol. 163, no. 4, pp. 245–255, 2010.

[12] D. Symons, R. Persaud, and H. Stanislaus, "Strength of inclined screw shear connections for timber and concrete composite construction," *Structural Engineer*, vol. 88, no. 1, pp. 25–32, 2010.

[13] M. Van der Linden, "Timber-concrete composite beams," *Heron*, vol. 44, no. 3, pp. 215–239, 1999.

[14] M. Fragiacomo, "Long-term behavior of timber-concrete composite beams. II: numerical analysis and simplified evaluation," *Journal of Structural Engineering*, vol. 132, no. 1, pp. 23–33, 2006.

[15] H. Corp, *Solutions of Shear Connectors*, Liechtenstein: Hilti Aktiengesellschaft, Schaan, Liechtenstein, 2016.

[16] M. Stepinac, V. Rajcic, and J. Barbalic, "Influence of long term load on timber-concrete composite systems," *Gradevinear*, vol. 67, no. 3, pp. 235–246, 2015.

[17] Z. Gan, Y. Sun, X. Sun, L. Zhou, and M. He, "Push-out performance of inclined screw shear connectors used in nail-laminated timber-concrete composite," *Construction and Building Materials*, vol. 366, Article ID 130175, 2023.

[18] J. H. J. O. Negrão, C. A. Leitão de Oliveira, F. M. Maia de Oliveira, and P. B. Cachim, "Glued composite timber-concrete beams. I: interlayer connection specimen tests," *Journal of Structural Engineering*, vol. 136, no. 10, pp. 1236–1245, 2010.

[19] E. E. Ducas, "Experimental study into the mechanics of inclined screw and perforated plate connections in timber-concrete composite floors," Undergraduate Research Report No. 1617RP016, Department of Civil Engineering, University of Bristol, Bristol, UK, 2017.

[20] V. De Araujo, F. Aguiar, P. Jardim et al., "Is cross-laminated timber (clt) a wood panel, a building, or a construction system? A systematic review on its functions, characteristics, performances, and applications," *Forests*, vol. 14, no. 2, p. 264, 2023.

[21] Cen, *Eurocode 5: Design of Timber Structures- Part 1- 1: General- Common Rules and Rules for Buildings*, BSI, Brussel, Europe, 2004.

[22] F. Moshiri, C. Gerber, H. R. Valipour, R. Shrestha, and K. I. Crews, "The predictive model for strength of inclined screws as shear connection in timber concrete composite floor," *Materials and Joints in Timber Structures*, vol. 9, pp. 443–453, 2014.

[23] H. Du, X. Hu, Z. Sun, and W. Fu, "Shear stiffness of inclined screws in timber–concrete composite beam with timber board interlayer," *Advances in Structural Engineering*, vol. 23, no. 16, pp. 3555–3565, 2020.

[24] M. A. Mirdad and Y. H. Chui, "Strength prediction of mass-timber panel concrete-composite connection with inclined screws and a gap," *Journal of Structural Engineering*, vol. 146, no. 8, Article ID 4020140, 2020.

[25] P. Gelfi, E. Giuriani, and A. Marini, "Stud shear connection design for composite concrete slab and wood beams," *Journal of Structural Engineering*, vol. 128, no. 12, pp. 1544–1550, 2002.

[26] Aci, *ACI CODE-318-19: Building Code Requirements for Structural Concrete*, American Concrete Institute, Farmington Hills, Michigan, USA, 2022.

[27] Cen, *Eurocode 2: Design of Concrete Structures- Part 1- 1: General- Rules and Rules for Buildings*, BSI, Brussel, Europe, 2004.

[28] W. M. Sebastian, J. Mudie, G. Cox, M. Piazza, R. Tomasi, and I. Giongo, "Insight into mechanics of externally indeterminate hardwood-concrete composite beams," *Construction and Building Materials*, vol. 102, no. 2, pp. 1029–1048, 2016.

[29] M. A. Bin Mohd Snin, *Development of Empirical Model of Shear Force Capacity and Stiffness of the Screw Connections in Timber – Concrete Composite Structures*, Ph.D. thesis, University of Bristol, Bristol, UK, 2021.

[30] Astm, *ASTM E8-13. Standard Test Methods for Tension Testing of Metallic Materials*, ASTM International, West Conshohocken, PA, USA, 2013.
[31] Astm, *ASTM C39-03. Standard Test Method for Compressive Strength of Cylindrical Concrete Specimens*, ASTM International, West Conshohocken, PA, USA, 2003.
[32] British Standards Institution (Bsi), *EN 26891:1991. Timber Structures. Joints Made with Mechanical Fasteners. General Principles for the Determination of Strength and Deformation Characteristic*, BSI, London, UK, 1991.
[33] L. Stehn and H. Johansson, "Ductility aspects in nailed glue laminated timber connection design," *Journal of Structural Engineering*, vol. 128, no. 3, pp. 382–389, 2002.
[34] Rcsc, *Specification for Structural Joints Using High- Strength Bolts*, Research Council on Structural Connections, Chicago, IL, USA, 2020.